Article

Deflected Talbot mediated overtone spectroscopy in near-infrared as a label-free sensor on a chip

aviad katiyi, and Alina Karabchevsky

ACS Sens., **Just Accepted Manuscript** • DOI: 10.1021/acssensors.0c00325 • Publication Date (Web): 08 May 2020

Deflected Talbot mediated overtone spectroscopy in near-infrared as a label-free sensor on a chip

Aviad Katiyi and Alina Karabchevsky*

School of Electrical and Computer Engineering, Ben-Gurion University of the Negev, Beer-Sheva 8410501, Israel.

Isle Katz Institute for Nanoscale Science & Technology, Ben-Gurion University of the Negev, Beer-Sheva 8410501, Israel

E-mail: alinak@bgu.ac.il

Abstract

Rapid, sensitive and reliable detection of aromatic amines - toxic manufacturing byproducts - have been previously achieved with molecular vibrations in Mid-infrared (Mid-IR) region. However, Mid-IR spectroscopic tools are hampered by a need to prepare the samples and the sensor cost. Here we develop an affordable label-free sensor on a chip, operating in near-infrared (NIR) for ultra-sensitive detection of absorption line signatures based on molecular vibrations overtones of aromatic amine *N*-Methylanilne probe molecule. We design a perforated silicon rib waveguide and fabricate it by milling cylindrical inclusions through the waveguide core. The molecular signatures were monitored when waveguides are embedded in toxic *N*-Methylanilne, experiencing deflected Talbot effect. We observed that when the Talbot effect is deflected, the absorption lines in NIR are enhanced despite the weakly absorbing nature of the probe molecules. This new spectroscopic strategy can potentially be extended to detect other common

toxic byproducts in a chip-scale label-free manner and to enhance the functionality of chemical monitoring.

Keywords

Molecular overtones, optical waveguide, multi-mode interference, near-infrared spectroscopy, integrated photonics

Multi-Mode Interference (MMI) devices have a growing interest in integrated optics[1,2] widely used for variety of applications such as communication,[3,4] sensing[5] and integrated photonics.[6,7] MMI devices has a characteristic Talbot pattern. This pattern was discovered in 1836 by Henry Fox Talbot[8] in a periodic structure such as diffraction grating which creates a self-imaging effect. By illuminating a diffraction grating, Talbot observed repetition of color bands. Later, in 1881, this effect was rediscovered and explained by Lord Rayleigh.[9] When the light passes through the periodic diffraction grating it creates an image of the grating at distance z_T which is named the *Talbot length*. Talbot effect also occurs in multimode (MM) waveguides.[10–12] However, in the MM waveguides the Talbot effect is related to the different propagation constants of the guided modes but not to the periodicity of the input source. When a guided wave is transmitted through a multimode optical waveguide, it creates wavefront replicates of a periodic perturbation pattern along the propagation direction of the guided wave.[13] This occurs due to the multimode interference effect. The MMI effect is used to minimize and improve the optical devices, such as Mach-Zehnder switches[14,15] and modulators,[16] and to enhance the functionality of integrated photonic circuits.

Our sensor is based on the MMI effect. It is important to note that MMI-based devices such as optical couplers have low propagation losses and allow for small device dimensions[13] which make them ideal for Mach-Zehnder interferometers[17] and other integrated photonic components. In addition, the multimode interference effect in a waveguide can be used for sensing applications. A sensor based on MMI can achieve a resolution of 5.41×10^{-5}

RIU.[18] Instead of using the MMI effect on a slab waveguide, the MMI structure can be also created out of slot waveguides. Due to the changes in the refractive index inside the slot, the output then is changed leading to the resolution of 9.8×10^{-5} RIU.[19] However, those structures behave as refractometers which is essentially lacks in specificity. In contrary, spectrometers operating in low energies in infra-red are specific since they able to identify molecular structure from the unique absorption lines. Despite the fundamental interest to understand the mechanism of absorption by molecular vibrations overtones, the probability of the overtone transition of $\Delta v > 1$ (v is the number of the energy level), is very small. The overtone absorption is order of magnitude smaller compared to the fundamental vibration absorption[20] which make the detection of the overtones absorption challenging.[21–23]

Here, we study the deflected Talbot effect realized in a weakly absorbing molecular medium. To understand the mechanism underlying the deflected Talbot effect in a weakly absorbing medium, we combined several disciplines, namely, the physics of guided wave optics, the waveguide with inclusions fabrication routines, the surface chemistry and the molecular overtone spectroscopy. We explore the overtone absorption by multimode interference (MMI) in multimode silicon rib waveguides and reveal that the deflected Talbot effect increases the probability of overtone transitions. Next, we investigate the influence of cylindrical inclusions in the guiding layer on the Talbot effect.

Experimental Section

Lumerical simulation. 3D simulations were performed using a commercial Maxwell solver: Lumerical - FDTD (Finite Difference Time Domain) solutions. A Gaussian beam, wavelength of 1.5 μm, radius of 4.75 μm, and divergence angle of 0.13 rad, was launched into a Silicon-On-Insulator (SOI) rib waveguide with slab height of 1.6 μm, strip height of 0.4 μm and width of 8 μm and waveguide length of 30 μm. The refractive indices of the silicon and silica are $n_{\mathrm{Si}}(1.5\ \mu\mathrm{m}) = 3.48$ and $n_{\mathrm{SiO_2}}(1.5\ \mu\mathrm{m}) = 1.444$. The waveguide was embedded in

N-methylaniline ($n_{\mathrm{NMA}}(1.5\ \mu\mathrm{m}) = 1.5712 + i8.931\text{E-}5$) in a distance of 10 μm from the input facet. The cross-section of the electric field in x-y and x-z plane was taken in the middle of the waveguide, $y = 0$ and $z = 1$ μm, respectively.

Waveguide fabrication. The rib waveguide was fabricated on Silicon-On-Insulator (SOI) wafer (Si Carrier 2 μm SiO_2 and 200 nm of Si). For the fabrication process, we used e-beam resist poly-methyl metacrylate (PMMA) 950K for writing the waveguides. After writing and developing the resist, we evaporated hard mask of aluminum with thickness of 50 nm via Electron Gun evaporator. Next, we soaked of the sample in acetone for 4 hours as lift off process, and we cleaned the sample with isopropanol (IPA). Eventually, we dry etched the sample with SF_6+Ar and O_2 which enable us to get a straight line and 90 degree waveguide wall. We removed the residue of the Al by a 400K developer.

Inclusion cluster fabrication. The inclusions of cylindrical shape were milled into the silicon guiding layer using a Helios focused ion beam (FIB). The holes were fabricated with depth of 2 μm and radius of 0.58 μm.

Spectroscopy on a waveguide. A broadband laser source (Fianium WL-SC-400-15), bandwidth of 450 nm to 2400 nm, was focused into a single mode fiber (1550BHP) using a X10 plan achromat objective (Olympus) with a numerical aperture of NA=0.25. The single-mode fiber was aligned to the waveguide using a 3D stage (3-Axis NanoMax Stage) and monitored by a Stereo Microscope (Zeiss Stemi SV6) for precise alignment. The transmitted spectra were collected using a multimode fiber into a optical spectrum analyzer (Yokogawa 6370D) at wavelength range of 1-1.7 μm and resolution of 1 nm.

Results and discussion

Molecular Overtone Transitions. Molecular vibrations overtones transitions can be excited in near-IR. Each molecular vibration transition has a different probability to occur

which is expressed by the oscillator strength. The oscillator strength f is proportional to the square of electric dipole transition moment:[24]

$$f = \left(\frac{4\pi m_e \nu_{ij}}{3e^2\hbar}\right)\left|\mu_{ij}\right|^2 \tag{1}$$

where m_e is the mass of an electron, $\hbar$ is the reduced Planck constant, ν_{ij} is the frequency for transition from state i to state j and μ_{ij} is the electric dipole transition moment which is defined as:

$$\mu_{ij} = < i|\mu|j > = \int \psi_i \mu \psi_j \, dr \tag{2}$$

where ψ is the wave function. The electric dipole moment μ is defined as:

$$\mu = \mu_0 + \left(\frac{\partial \mu}{\partial r}\right)_0 r + \frac{1}{2}\left(\frac{\partial^2 \mu}{\partial r^2}\right)_0 r^2 + ... \tag{3}$$

where μ_0 is the dipole moment at $r = 0$ where r is the displacement and 0 indicates that the derivatives are at the equilibrium bond length (Detailed description of oscillator strength can be found in the Supplementary Materials file). From Eq. S-10 in the Supplementary Materials, one can see that the probability of the overtone vibration is order of magnitude smaller compared to the probability fundamental vibration[20] which makes it hard to identify. For this reason, here we propose to enhance the overtone transition probability by induced deflected Talbot effect on perforated optical waveguides with inclusions of cylindrical shape.

In order to investigate the influence of the inclusions on Talbot effect, we study a Silicon-On-Insulator (SOI) nanostrip rib waveguide with 5 nm Ta_2O_5 overlayer, which acts as a capping layer, having cluster made of cylindrical inclusions in the guiding layer which is shown in Fig. 1. We choose a square configuration for the holes cluster due to the growing interest of quadrumers for different fundamental phenomena.[25] A cylindrical shape was chosen for the inclusions due to the easy fabrication process compared to other shapes. To observe Talbot effect by a multimode interference, we modeled the waveguide with height of

1.6 μm and nanostrip height of 400 nm and inclusion diameter of 1.12 μm as shown in Fig.1.

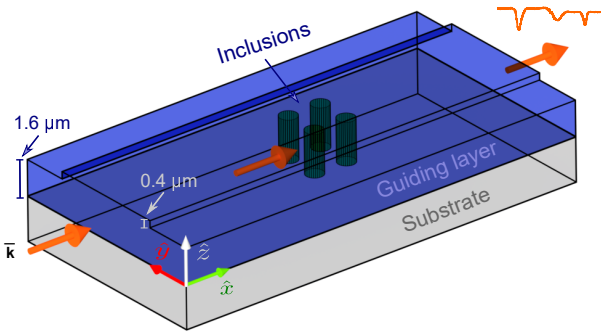

Figure 1: Schematic of the dielectric rib waveguide with silicon guiding layer on silica substrate with cluster of inclusions of cylindrical shape.

Using Lumerical - FDTD software, we modeled the waveguide when the inclusions are embedded in different media: air and weakly absorbing media of *N*-methylaniline (NMA) molecule.[26] A Gaussian beam, with wavelength of 1.5 μm, radius of 4.75 μm and divergence angle of 0.13 rad, was launched into the waveguide. The inclusions were engraved at a distance of 20 μm from the input facet. We explored the conditions for the deflected Talbot regime in x-y and x-z waveguide planes and its influence on molecular overtone transitions. Due to the propagation of number of modes in a multimode waveguide, a wavefront replicates the periodic perturbation pattern along the propagation. When the dielectric perturbation occurs in a waveguide, some of the power transfers to other modes which creates the deflected Talbot effect.

First, we investigated the influence of the inclusions at the x-z plane of the waveguide. Figure 2a shows a schematic cross-section in the center of the waveguide at x-z plane. Due to the multimode interference, a self-imaging Talbot effect occurs in the silicon rib waveguide (Fig. 2b). When the cylindrical inclusions cluster placed inside the core, the deflected Talbot effect (Figs 2c-d) occurs when the guiding layer is embedded in air and in weakly absorbing medium with dispersion of *N*-methylaniline,[22,26] respectively, which creates perturbation along the propagation direction of the waveguide. Next, we investigated the influence of the

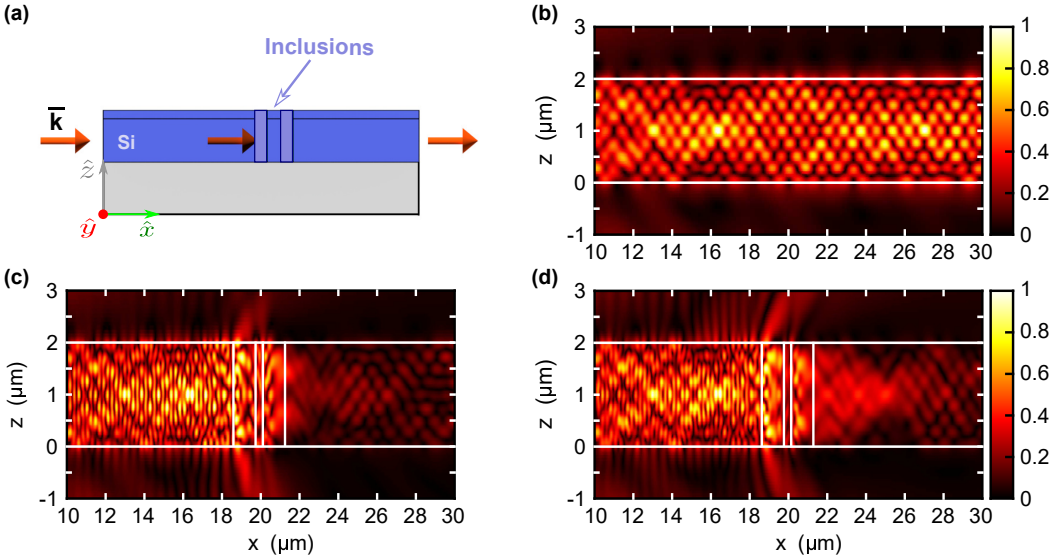

Figure 2: (a) Schematic of the cross-section in the center of the waveguide, x-z plane ($y = 0\ \mu$m). Evolution of the electric field when waveguide embedded in (b) air without inclusions, (c) air with inclusions and (d) N-methylaniline, $n_{\mathrm{NMA}} = 1.5712 + i8.931\text{E-}5$, with inclusions.

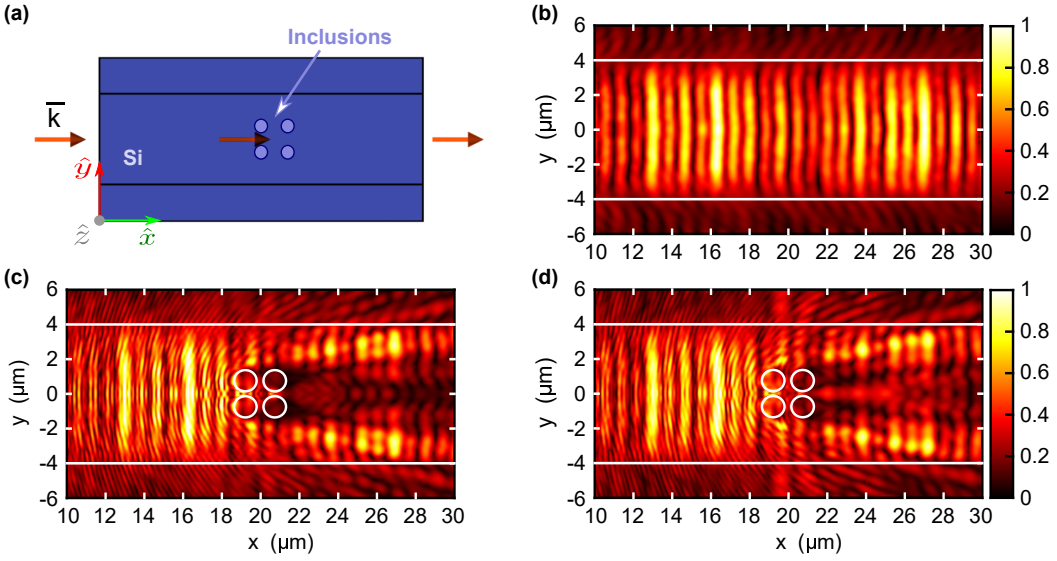

Figure 3: (a) Schematic of the cross-section in the center of the waveguide, x-y plane ($z = 1\ \mu$m). Evolution of the electric field when waveguide embedded in (b) air without inclusions, (c) air with inclusions and (d) N-methylaniline, $n_{\mathrm{NMA}} = 1.5712 + i8.931\text{E-}5$, with inclusions.

inclusions at the x-y plane of the waveguide. Figure 3a shows a schematic cross-section in the center of the waveguide at x-y plane. Figure 3b shows the Talbot effect in the silicon rib waveguide as a deformation of the field along the propagation. A perturbation appears along the propagation direction in the waveguide (Figs. 3c-d) caused by the introduced inclusions cluster in the guiding layer embedded in air and in *N*-methylaniline, respectively. We notice a leakage beyond the waveguide strip confinement. Figures 2-3 show that some power transfers to the other modes and the Talbot effect becomes deflected due to the dielectric perturbation of cylindrical shape (The evolution of the guided modes are shown in Supplementary materials).

For the experiment, we first fabricated and characterized the silicon rib waveguides. Figure 4a shows a scanning electron micrograph image of fabricated rib waveguides (top view) without inclusions. Next, the Talbot effect was deflected by cylindrical inclusions cluster milled into the guiding layer with focused ion beam (FIB) with a depth of 2 μm and a radius of 580 nm. Figure 4b shows a scanning electron micrograph image of the zoomed area on fabricated inclusions cluster (top view). The waveguides were characterized and tested using the inline waveguide measurement set-up, as described in the experimental section. Figure 4c shows photograph of the inline set-up with fiber in-coupled rib waveguide aligned on 3D stage. Fiber-out is collecting the output signal from the waveguide into the optical sepctrum analyser (OSA) - not shown.

To further explore the influence of the deflected Talbot regime on the overtone molecular absorption on the waveguide, we constructed the experimental set-up shown in Fig. 5a. We used a red light of 80 mW. Therefore, partially such a high-power light can be guided in the waveguide. It allows for the visualization of the waveguide lines and facilitates the alignment. Next, a broadband laser source was coupled to a single-mode fiber (SMF1550). The fiber was placed on a piezo-electric stage for precise and accurate inspection. The output signal was collected by a multi-mode fiber into an optical spectrum analyzer (OSA). We dropped 12 μL of *N*-methylaniline onto the inclusions cluster shown in Fig. 4c resulting in the spectra

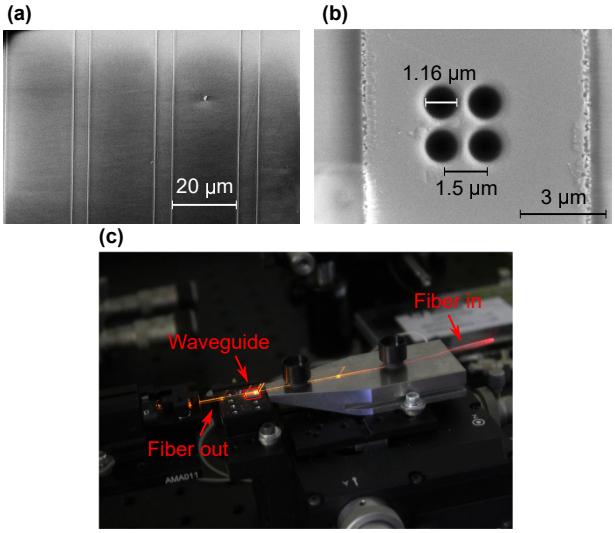

Figure 4: (a) Scanning electron microscope (SEM) image of the rib waveguide. (b) Scanning electron microscope (SEM) image of the fabricated inclusions on the rib waveguide. (c) Photograph of the in-line experimental set-up.

shown in Fig. 5b (blue curve). For comparison, the laser was coupled to the reference waveguide (with no inclusions) with *N*-methylaniline resulting in spectra shown in Fig. 5b (red curve). Figures 5c-d show upper view of the illuminated waveguide.

Figure 5b shows transmittance spectrum of *N*-methylaniline on rib waveguide with and without inclusions at broad wavelengths range of 1.3-1.6 μm. The absorption of the N-H bond in *N*-methylaniline is clearly see around 1.5 μm on the waveguide with the inclusions. The absorption of *N*-methylaniline when dripped onto the waveguide surface and filled in the inclusions is approximately 3.5 dB compared to dripped *N*-methylaniline on a waveguide without the inclusions. It shows that in deflected Talbot regime caused by the inclusions we enhance the absorption effect of *N*-methylaniline probe molecule. Figure 5d shows the far-field scattering effect caused by the cylindrical inclusions compared to the scattering in the reference waveguide, shown in Fig. 5c which fit the simulation results shown in Fig. 3b and Fig. 3d.

We noticed that dielectric perturbations such as cylindrical holes, enhance the absorption when the hole diameter is comparable to the incident wavelength. This can be explained by the scattering effect.

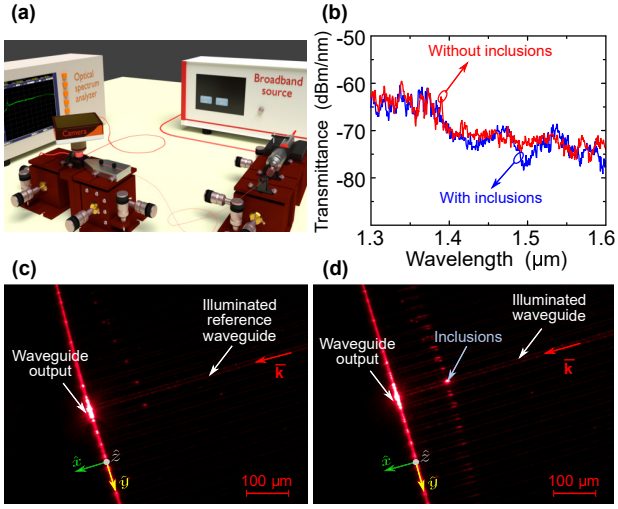

Figure 5: (a) Artistic impression of the experimental set-up. (b) Measured transmittance spectra with OSA on reference waveguide (red curve) and on waveguide with cylindrical inclusions cluster (blue curve). Note, both waveguides were embedded in N-Methylaniline medium. Top view of the waveguides captured with an optical microscope (c) The reference waveguide. (d) The waveguide with fabricated inclusions.

2D Scattering from Cylinder Embedded in the Waveguide Core. The enhanced absorption of N-methylaniline overtones can be explained by the multiple scattering events.[26,27] One can explain the resonant elastic scattering of light by a chain of coherent absorption and re-emission events. Simply put, the photons are re-emitted in random directions because the wave-vector is not conserved by the system for the lack of translational symmetry. The resonant scattering results in a significant increase of the mean trajectory of photons travelling through the guide. However, the actual scattering of a waveguide mode by a finite cylinder with height of $H \sim \lambda$ and diameter of $D \sim \lambda$ cannot be solved analytically. Therefore, for describing the scattering effect by cylinders in waveguide core, we will ignore the height restriction of the cylinder and illuminate it with a planar wave.

In case of TE mode when the electric field is parallel to the xz plane, the scattered fields of a single cylinder (shown in Fig. 6a) is defined as:[28]

$$\mathbf{E}_s = -\sum_{n=-\infty}^{\infty} E_n \left[b_{nI} \mathbf{N}_n^{(3)} + i a_{nI} \mathbf{M}_n^{(3)} \right] \tag{4}$$

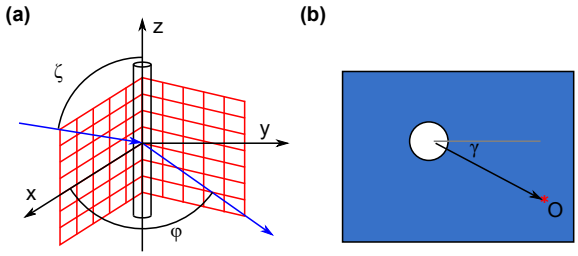

Figure 6: (a) A long cylinder illuminated by a plane wave. (b) Top view of the cylindrical hole.

$$\mathbf{H}_s = i\frac{k}{\omega\mu}\sum_{n=-\infty}^{\infty} E_n\left[b_{nI}\mathbf{M}_n^{(3)} + ia_{nI}\mathbf{N}_n^{(3)}\right] \tag{5}$$

where $E_n = E_0(-i)^n/(k\sin\zeta)$ and $\mathbf{M}_n^{(3)}, \mathbf{N}_n^{(3)}$ are the proper cylindrical vector harmonics[28] which are given by:

$$\mathbf{M}_n^{(3)} = \nabla \times (\hat{z}\psi_n) \tag{6}$$

$$\mathbf{N}_n^{(3)} = \frac{\nabla\times\mathbf{M}_n}{k} \tag{7}$$

where ψ_n is the generation function which is defined as:

$$\psi_n = H_n^{(1)}(kr\sin\zeta)e^{in\varphi}e^{-ikz\cos\zeta} \tag{8}$$

where k is the wavenumber and $H_n^{(1)}$ is the Hankel function of the first kind - $H_n^{(1)} = J_n + iY_n$.

Using the continuity equations for E and H at the cylinder boundary ($r = a$), we obtain the two coefficients:

$$a_{nI} = \frac{C_nV_n - B_nD_n}{W_nV_n + iD_n{}^2}$$
$$b_{nI} = \frac{W_nB_n + iC_nD_n}{W_nV_n + iD_n{}^2}.$$

where the auxiliary functions are defined as:

$$B_n = \xi\left[m^2\xi J'_n(\eta)J_n(\xi) - \eta J_n(\eta)J'_n(\xi)\right]$$
$$C_n = n\cos(\zeta)J_n(\eta)J_n(\xi)\left(\frac{\xi^2}{\eta^2} - 1\right)$$
$$D_n = n\cos(\zeta)\eta J_n(\eta)H_n^{(1)}(\xi)\left(\frac{\xi^2}{\eta^2} - 1\right)$$
$$W_n = i\xi\left[\eta J_n(\eta)H_n^{(1)\prime}(\xi) - \eta H_n^{(1)}(\xi)J'_n(\eta)\right]$$
$$V_n = \xi\left[m^2\xi J'_n(\eta)H_n^{(1)\prime}(\xi) - \eta H_n^{(1)\prime}(\xi)J_n(\eta)\right]$$

and

$$\xi = ka\sin\zeta \qquad \eta = ka\sqrt{m^2 - \cos(\zeta^2)}$$

where m is the relative refractive index of the medium filling the cylinder ($m = \frac{n_a + i\kappa_a}{n_{\mathrm{wg}}}$) and a is the cylinder radius.

In case of a waveguide, the incident illumination is at normal incident to the inclusions ($\zeta = 90$), hence a_{nI} is equal to zero. Therefore, b_{nI} can be calculated as:

$$b_{nI} = \frac{J_n(mx)J'_n(x) - mJ'_n(mx)J_n(x)}{J_n(mx)H_n^{(1)\prime}(x) - mJ'_n(mx)H_n^{(1)}(x)} \tag{9}$$

For a finite cylinder, the correction factor is given by[29] $f_c = \frac{2\sin(kLA)}{kLA}$ where $A = \cos\zeta + \sin\theta\cos\phi$ and L is half of the cylinder length. This factor provides the spectral correction which depend on the cylinder length. However, it does not consider a space dependence of the field along the cylinder axes.

Using this simplified model, we can estimate the effect of the inclusion cluster. Using a single scattering model, the scattered field at an arbitrary point O is described as the sum of scattered field of each hole.

$$\mathbf{E}_{s(t)} = \sum_{n=1}^{4}\mathbf{E}_{sn}(\gamma_n, |\mathbf{r}_O - \mathbf{r}_n|) \tag{10}$$

where n is the hole number and γ_n is the angle from hole to point O.

The scattered field $\mathbf{E}_{s(t)}$ from the whole cluster of inclusions leads to the enhanced absorption when the hole diameter is comparable to the incident wavelength. The scattering transfers an energy to the high order modes which have larger interaction with the surrounding. The scattering enhances the sensitivity of the waveguide, allowing us the identify the unique absorption lines of the molecule.

Conclusions

In conclusion, we have presented a waveguide system experiencing deflected Talbot effect due to the appearance of perturbations of cylindrical shape in waveguide core embedded in weakly absorbing medium N-Methylaniline.[26] We fabricated the waveguides on SOI platform and milled inclusions in them using FIB technique. We found that the deflected Talbot effect on a waveguide enhances the absorption of molecular transitions overtones. Specifically, the absorption line of N-H bond of N-Methylaniline excited around 1.5 μm experienced a drop of 3.5 dB as compared to unperturbed by inclusions waveguide. In addition, we noticed that dielectric perturbations such as cylindrical holes, enhance the absorption when the hole diameter is comparable to the incident wavelength , due to the scattering effect. This paves the way for integrated spectrometers in which the enhancement of the weak absorption occurs due to the perturbation in waveguide core.

Author Information

Corresponding Author

*E-mail: alinak@bgu.ac.il.

Notes

The authors declare no competing financial interest.

Acknowledgement

Authors acknowledge Dr. Ioseph Gurwich for fruitful discussion.

Supporting Information Available

The following files are available free of charge.

- Deflected Talbot mediated overtone spectroscopy in near-infrared as a label-free sensor on a chip - Supporting Information

References

(1) Yin, R.; Jiang, X.; Yang, J.; Wang, M. Structure with improved self-imaging in its graded-index multimode interference region. *JOSA B* **2002**, *19*, 1301–1303.

(2) Khalil, D.; Yehia, A. Two-dimensional multimode interference in integrated optical structures. *Journal of Optics A: Pure and Applied Optics* **2003**, *6*, 137.

(3) Ota, M.; Sumimura, A.; Fukuhara, M.; Ishii, Y.; Fukuda, M. Plasmonic-multimode-interference-based logic circuit with simple phase adjustment. *Scientific reports* **2016**, *6*, 24546.

(4) Lierstuen, L.; Sudbo, A. 8-channel wavelength division multiplexer based on multimode interference couplers. *IEEE Photonics Technology Letters* **1995**, *7*, 1034–1036.

(5) Wan, N. H.; Meng, F.; Schröder, T.; Shiue, R.-J.; Chen, E. H.; Englund, D. High-resolution optical spectroscopy using multimode interference in a compact tapered fibre. *Nature communications* **2015**, *6*, 7762.

(6) Peruzzo, A.; Laing, A.; Politi, A.; Rudolph, T.; O'brien, J. L. Multimode quantum

interference of photons in multiport integrated devices. *Nature communications* **2011**, *2*, 224.

(7) Geints, Y. E.; Minin, O. V.; Minin, I. V.; Zemlyanov, A. A. Self-images contrast enhancement for displacement Talbot lithography by means of composite mesoscale amplitude-phase masks. *Journal of Optics* **2019**, *22*, 015002.

(8) Talbot, H. F. LXXVI. Facts relating to optical science. No. IV. *The London and Edinburgh Philosophical Magazine and Journal of Science* **1836**, *9*, 401–407.

(9) Rayleigh, L. *The London, Edinburgh, and Dublin Philosophical Magazine and Journal of Science* **1881**, *11*, 196–205.

(10) Bryngdahl, O. Image formation using self-imaging techniques. *JOSA* **1973**, *63*, 416–419.

(11) Ulrich, R. Light-propagation and imaging in planar optical waveguides. *Nouvelle Revue d'Optique* **1975**, *6*, 253.

(12) Praxmeyer, L.; Wódkiewicz, K. Talbot effect in cylindrical waveguides. *Optics communications* **2006**, *268*, 215–225.

(13) Soldano, L. B.; Pennings, E. C. Optical multi-mode interference devices based on self-imaging: principles and applications. *Journal of lightwave technology* **1995**, *13*, 615–627.

(14) Bachmann, M.; Smit, M.; Besse, P.; Gini, E.; Melchior, H.; Soldano, L. Polarization-insensitive low-voltage optical waveguide switch using InGaAsP/InP four-port Mach-Zehnder interferometer. Optical Fiber Communication Conference. 1993; p TuH3.

(15) Agrawal, N.; Weinert, C.; Ehrke, H.-J.; Mekonnen, G.; Franke, D.; Bornholdt, C.; Langenhorst, R. Fast 2 x 2 Mach-Zehnder optical space switches using InGaAsP-InP multiquantum-well structures. *IEEE photonics technology letters* **1995**, *7*, 644–645.

(16) Zucker, J.; Jones, K.; Chiu, T.; Tell, B.; Brown-Goebeler, K. Strained quantum wells for polarization-independent electrooptic waveguide switches. *Journal of lightwave technology* **1992**, *10*, 1926–1930.

(17) Jenkins, R.; Devereux, R.; Heaton, J. A novel waveguide Mach-Zehnder interferometer based on multimode interference phenomena. *Optics communications* **1994**, *110*, 410–424.

(18) Wang, J.; Jin, Y.; Zhao, Y.; Dong, X. Refractive index sensor based on all-fiber multimode interference. *Optik-International Journal for Light and Electron Optics* **2013**, *124*, 1845–1848.

(19) Mayeh, M.; Viegas, J.; Srinivasan, P.; Marques, P.; Santos, J. L.; Johnson, E. G.; Farahi, F. Design and fabrication of slotted multimode interference devices for chemical and biological sensing. *Journal of Sensors* **2009**, *2009*.

(20) Stuart, B. *Infrared spectroscopy: Fundamentals and applications*; John Wiley & Sons, Ltd.: Sussex, 2004.

(21) Struve, W. S. *Fundamentals of molecular spectroscopy*; Wiley New York, 1989.

(22) Katiyi, A.; Karabchevsky, A. Figure of merit of all-dielectric waveguide structures for absorption overtone spectroscopy. *Journal of Lightwave Technology* **2017**, *35*, 2902–2908.

(23) Borovkova, O.; Ignatyeva, D.; Sekatskii, S.; Karabchevsky, A.; Belotelov, V. High-Q surface electromagnetic wave resonance excitation in magnetophotonic crystals for supersensitive detection of weak light absorption in the near-infrared. *Photonics Research* **2020**, *8*, 57–64.

(24) Atkins, P. W.; Friedman, R. S. *Molecular quantum mechanics*; Oxford university press, 2011.

(25) Terekhov, P. D.; Evlyukhin, A. B.; Redka, D.; Volkov, V. S.; Shalin, A. S.; Karabchevsky, A. Magnetic Octupole Response of Dielectric Quadrumers. *Laser & Photonics Reviews*

(26) Karabchevsky, A.; Kavokin, A. Giant absorption of light by molecular vibrations on a chip. *Scientific reports* **2016**, *6*, 21201.

(27) Karabchevsky, A.; Katiyi, A.; Bin Abdul Khudus, M. I. M.; Kavokin, A. V. Tuning the Near-Infrared Absorption of Aromatic Amines on Tapered Fibers Sculptured with Gold Nanoparticles. *ACS Photonics* **2018**, *5*, 2200–2207.

(28) Bohren, C. F.; Huffman, D. R. *Absorption and scattering of light by small particles*; John Wiley & Sons, 2008.

(29) Hulst, H. C.; van de Hulst, H. C. *Light scattering by small particles*; Courier Corporation, 1981.

Graphical TOC Entry